Available online at www.sciencedirect.com
ScienceDirect
Journal of Magnetic Resonance 185 (2007) 19–27
JMR Journal of Magnetic Resonance
www.elsevier.com/locate/jmr

Application of a portable nuclear magnetic resonance surface probe to porous media

Andriy Marko, Bernd Wolter, Walter Arnold *

Fraunhofer Institute for Non-Destructive Testing (IZFP), Building E 3.1, University, D 66123 Saarbrücken, Germany

Received 21 September 2006; revised 20 October 2006
Available online 30 November 2006

Abstract

A portable nuclear magnetic resonance (NMR) surface probe was used to determine the time-dependent self-diffusion coefficient $D(t)$ of water molecules in two fluid-filled porous media. The measuring equipment and the inhomogeneous magnetic fields in the sensitive volume of the probe are described. It is discussed how to evaluate $D(t)$ using a surface probe from the primary and stimulated echoes generated in three-pulse experiments. Furthermore, the evaluation of $D(t)$ allows one to determine the geometrical structure of porous materials.

Keywords: Nuclear magnetic resonance (NMR); One-sided access NMR; Porous media; Diffusion coefficient

1. Introduction

New nuclear magnetic resonance (NMR) devices, especially those which can be used for on-site and on-line measurements, have been intensively developed in the last decade. Special attention was paid to ''Inside-out'' or ''One-sided access'' (OSA) NMR techniques which allow measurements on components external to the apparatus. NMR well-logging instruments [1,2] and portable NMR surface probes [3–6] are examples of this technique. The applications of the NMR surface probe have been substantially extended in recent years, particularly for mobile on-site material characterization. Quality control of diverse rubber products, such as car tires and rubber pipes, can be performed non-destructively by this technique. The monitoring of adhesive curing in glass–metal compounds and other adhesive bonds has been reported [7,8]. The OSA technique is a suitable method to characterize the durability of building materials even if large components have to be examined, and it can also be used to monitor the early age strength development of concrete [9]. A further application is the survey of cultural-heritage objects, such as ancient-fresco painted walls and antique books [10,11]. Based on the portable NMR surface probe, magnetic resonance imaging (MRI) is under development [12–14] and highly resolved NMR spectra have been obtained [15,16].

Similarly to the standard NMR technique and the NMR well-logging equipment, which are used to characterize porous structures and rock formations in order to provide information about their porosity, saturation, characteristic pore size, and permeability [17–19], a portable NMR surface probe can be applied for the structural characterization of fluid-filled porous media [20]. Generally, the measurements of the relaxation times T_1 and T_2 for which $T_{1,2} = \rho_{1,2} a$ holds, cannot be used for an unambiguous characterization of the size a of the pores. The surface absorption coefficient ρ is a distinct material property and in many cases it is not known a priori. This problem can be avoided by carrying out diffusion measurements. Since the discovery of the links between diffusion and NMR signals [21–23], much work has been done to find relations between NMR signals obtained in homogeneous and inhomogeneous fields, and the geometrical and the transport parameters of disordered media [18,19,24–31].

* Corresponding author. Fax: +49 681 9302 5920.
E-mail address: walter.arnold@izfp.fraunhofer.de (W. Arnold).

1090-7807/$ - see front matter © 2006 Elsevier Inc. All rights reserved.
doi:10.1016/j.jmr.2006.10.009

Using a bar-magnet in the so-called NMR-MOUSE, a constant relaxation method for measuring the self-diffusion constant D has been implemented recently [32]. However, for the structural characterization of porous media, the time-dependent self-diffusion coefficient $D(t)$ which is linked with the mean squared displacement (MSD) of the liquid molecules in a restricted pore volume is the desired value. $D(t)$ is typically measured in pulsed field-gradient spin-echo (PFGSE) experiments by analyzing the echo magnitude for different gradient pulse durations. In the presence of a strong permanent static gradient, the MSD of liquid molecules can be measured in a three-pulse stimulated echo experiment [18] without using a gradient pulse-coil in the probe, which can cause additional technical problems [33].

The influence of diffusion on the echo signals, as well as the determination of diffusion parameters from the received signals by the inside-out NMR technique have shown a considerable amount of complications which are caused not only by a reduced signal-to-noise ratio in comparison to the standard NMR technique, but also by the inhomogeneity of the static magnetic field $\mathbf{B}$ as well as the radio-frequency field $\mathbf{B}_1$ across the sensitive volume [34,35]. Furthermore, the orthogonality between both fields, and the condition that the polarizing field-offset ΔB is much smaller than B_1, are not always fulfilled. Therefore, for signal calculations obtained with the portable NMR probe, the gradients of the static and radio-frequency fields, as well as their complex geometry have to be taken into account [6,36].

In this paper measurements of self-diffusion over a large time scale in liquid-filled porous media by means of a portable NMR surface probe are reported. For this purpose the magnetic fields of the probe are approximated by analytical expressions in the sensitive volume. Extending previous theoretical work by one of the authors which is based on the Greens function formalism to calculate the transversal magnetization in unbounded and bounded volumes [37] and using theoretical works of other authors [18,23,27–30], it is shown that it is possible to evaluate $D(t)$ from the echo signals generated by three-pulse sequences measuring the amplitude ratios between the two-pulse and three-pulse echoes. The limits are described within which this kind of diffusion measurement can be used. The experimentally obtained time dependence of the diffusion coefficient is used to determine the surface-to-volume ratio S/V, the formation factor F, and the permeability k [38] for two porous media: water-filled glass beads and a water-filled SiO_2 powder. The obtained results for the S/V parameters agree well with the values of the specific surface in both porous media.

2. Description of the measuring equipment

The portable NMR probe has the size $250 \times 240 \times 260\ \text{mm}^3$ mounted in a copper and aluminum housing. It consists of an rf-transmitting and receiving pancake coil, a bipolar magnet assembly and a high-voltage capacitor (see Fig. 1a). The static magnetic field $\mathbf{B}(\mathbf{r})$ is created by several bar NdFeB magnets with the energy density of $\approx 7.96 \times 10^3\ \text{J/m}^3$ (=38 MGOe in cgs units as given by the manufacturer) and connected by an iron yoke forming an U-shape assembly. The magnetic field gradient is about 3 T/m (details see in Appendix A). By using an optimized magnet design, the magnet weight was minimized (total weight of the probe 38.5 kg) and a measuring depth up to several centimeters was achieved [4]. A flat pancake Cu-coil (2 mm wire Ø, 100 mm coil Ø, 7 turns), which is connected to the high-voltage capacitor, generates a linearly polarized alternating magnetic field $\mathbf{B}_1(\mathbf{r}, t)$ parallel to the coil axis. The resonant circuit formed by the capacitor and the coil is tunable between 5.2 and 9 MHz. In the present study a resonance frequency of $\nu = 5.2$ MHz was used which corresponds to a measuring depth of 27 mm. In order to generate a substantial rf-magnetic field, the electrical pulse power fed into the resonance circuit can be as high as 30 kW. It is generated by a specially developed miniature

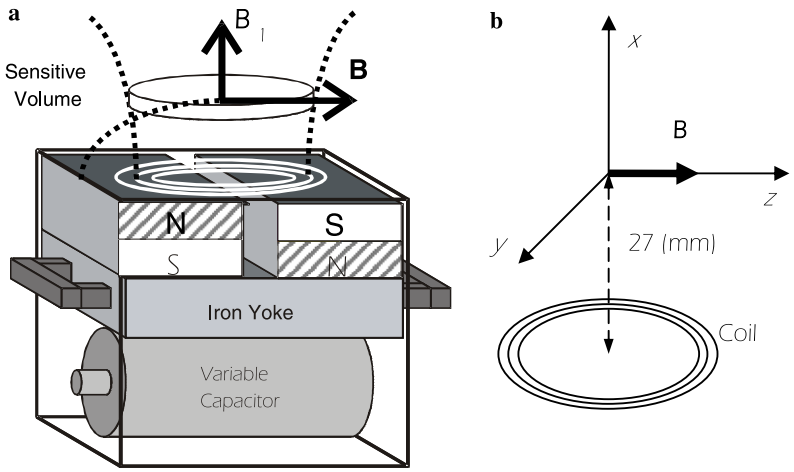

Fig. 1. (a) Schematic diagram of the portable probe. The static magnetic field $\mathbf{B}(\mathbf{r})$ is created by permanent magnets and the rf-field $\mathbf{B}_1(\mathbf{r}, t)$ by a pancake coil with seven turns. The center of the sensitive volume is 27 mm from the probe surface for a frequency of 5.2 MHz; (b) the coordinate system with the origin in the center of the sensitive volume.

rf amplifier on a standard board. Rf pulses were typically several microseconds long. The dimensions of the portable electronic sub-unit are $430 \times 430 \times 200\ \mathrm{mm}^3$, with a mass of 15 kg. It can be powered by line voltages of 110 or 220 V with an overall consumption of 100 W or for 120 min by batteries. The portable electronic sub-unit consists of a frequency synthesizer with a 80 MHz master clock, a pulse programmer, a low-impedance output stage, a 3-port switch with an impedance-matching network with tunable varactor diode, active and passive dampers, a low-noise pre-amplifier with a variable bandwidth between 50 and 500 kHz, a frequency-variable demodulator, an A/D-converter with an 80 MHz digitization rate, and finally a computer and a touch-screen display.

The static magnetic field $\mathbf{B}(\mathbf{r})$ can be calculated numerically [6,36]. Its amplitude along the axis of the coil decreases with the distance x from the probe surface and it reaches at $x = 27$ mm the value B_0 for which the angular velocity of proton magnetic-moment precession $\gamma_p B_0$ is equal to the angular frequency of the rf-field: $\gamma_p B_0 = \omega_0 = 2\pi\nu = 32.6725$ (rad/μs). Here γ_p is the proton gyromagnetic ratio.

The center of the sensitive volume is the origin for a Cartesian coordinate system (see Fig. 1b). The x-axis of this coordinate system is parallel to the symmetry axis of the rf-coil, and the z-axis is oriented horizontally from the north to the south pole of the U-shaped magnet assembly. The static magnetic field $\mathbf{B}(\mathbf{r})$ and the rf-field $\mathbf{B}_1(\mathbf{r}, t)$ can be approximated near the center of the sensitive volume by a polynomial function which reflects the symmetry of the magnet and the coil (see Appendix A).

3. Estimation of diffusion parameters

In the following a system of isolated spins placed in the magnetic fields, which are described by Eqs. (A1) and (A2) of Appendix A is considered. Each spin has the effective magnetic moment $\mu_0 = \mu_B^2 B(\mathbf{r})/k_B T$ oriented along the static magnetic field $\mathbf{B}(\mathbf{r})$ in the equilibrium state. Here μ_B is the Bohr magneton, k_B is the Boltzmann constant, and T is the temperature. For the three-pulse experiments the echo magnitudes can be calculated by considering the dynamics of proton magnetic moments under the action of the applied inhomogeneous magnetic fields (see Appendix B), which has been described earlier by various groups based on the well-known rotation matrices formalism [6]. In the cases of a more complicated sequence such as CPMG, the selection of coherent pathways into which the magnetization dynamics is decomposed, has been used to evaluate echo amplitudes [35]. The primary echo magnitude, which is built up after two t_p-long pulses with the delay τ_1 between them, is determined by the following expression:

$$M(t_p, \tau_1) = \mu_0 n \exp\left(-\frac{2\tau_1}{T_2}\right) \int I_1(\mathbf{r}, t_p) \times \exp\left(-\gamma_p^2 \mathbf{G}^2(\mathbf{r}) Z_{\tau_1}(\tau_1)\right) \mathrm{d}v. \quad (1)$$

Here, n is the density of the protons and $n\,\mathrm{d}v$ is the total number of protons in the volume $\mathrm{d}v$. $I_1(\mathbf{r}, t_p)$ can be called the volume excitation function for the first echo. It is determined by

$$I_1(\mathbf{r}, t_p) = \frac{1}{2}\big(c(\mathbf{r}, t_p) - I(\mathbf{r}, t_p)\big)\big(O(\mathbf{r}, t_p) + \mathrm{i}s(\mathbf{r}, t_p)\big). \quad (2)$$

It shows the spatial distribution of magnitude and phase of the proton magnetization in the sample. The diffusion relaxation factor $\exp(-\gamma_p^2 \mathbf{G}^2(\mathbf{r}) Z_{\tau_1}(\tau_1))$ in Eq. (1) depends on the local value of the gradient $\mathbf{G}(\mathbf{r})$ and on the function $Z_\tau(t)$ which represents the thermal molecular motion [18]. The function $Z_\tau(t)$ is determined by the following expression:

$$Z_\tau(t) = \frac{1}{6}\left\{\int_0^\tau \int_t^{t+\tau} \big\langle \mathbf{r}^2(|t'' - t'|)\big\rangle \mathrm{d}t'\,\mathrm{d}t'' - \int_0^\tau \int_0^\tau \big\langle \mathbf{r}^2(|t'' - t'|)\big\rangle \mathrm{d}t'\,\mathrm{d}t''\right\}. \quad (3)$$

After the third t_p-long pulse, which follows the second pulse after the delay τ_2, the echo magnetization is determined by

$$M(t_p, \tau_1, \tau_2) \approx \mu_0 n \exp\left(-\frac{2\tau_1}{T_2} - \frac{\tau_2}{T_1}\right) \int I_2(\mathbf{r}, t_p) \times \exp\left(-\gamma_p^2 \mathbf{G}^2(\mathbf{r}) Z_{\tau_1}(\tau_1 + \tau_2)\right) \mathrm{d}v. \quad (4)$$

Here $I_2(\mathbf{r}, t_p)$ is the volume excitation function of the stimulated echo

$$I_2(\mathbf{r}, t_p) = -\tfrac{1}{2}\big(O(\mathbf{r}, t_p) + \mathrm{i}\, s(\mathbf{r}, t_p)\big)\big(O^2(\mathbf{r}, t_p) + s^2(\mathbf{r}, t_p)\big). \quad (5)$$

The echo magnitude is the superposition of the contributions from the locally excited volumes which in general can be attenuated by their own diffusion factor. In the following the normalized magnitudes of the primary and the stimulated echoes, $M(t_p, 0)/(\mu_0 n)$ and $M(t_p, 0, 0)/(\mu_0 n)$, respectively, were numerically simulated as functions of the pulse length t_p for the magnetic fields of the portable probe (see Fig. 2a).

The results (1)–(5) are used in order to extract the diffusion parameters from the measured echo signals by using an approximation. The in- and out-of-phase voltage induced in the coil from the sample with the complex magnetization density $m(\mathbf{r}, t)$ can be described by the complex function $V(t)$ [34]

$$V(t) = \frac{2}{I_c} \int \omega_1(\mathbf{r}) B(\mathbf{r}) m(\mathbf{r}, t)\, \mathrm{d}v. \quad (6)$$

Here, I_c is the current needed in the coil to give rise to $B_1(\mathbf{r})$ in the sample. Next the voltage amplitudes of the primary and stimulated echo signals are described as $V(t_p, \tau_1)$ and $V(t_p, \tau_1, \tau_2)$, respectively. We determine the logarithm of the ratio between the absolute values of the signals of the stimulated and the primary echoes $\ln|V(t_p, \tau_1, \tau_2)/V(t_p, \tau_1)|$. With Eqs. (1) and (4) this quantity can be calculated

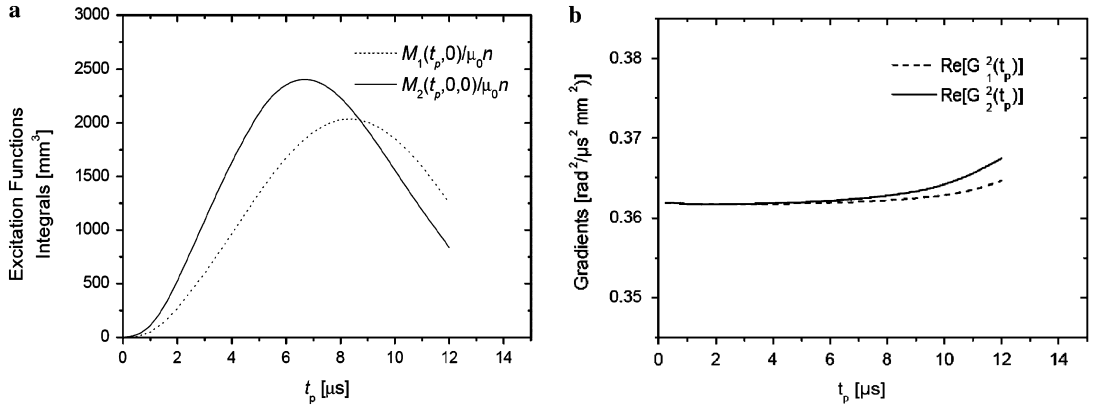

Fig. 2. (a) Amplitude of the primary and stimulated echoes as a function of the rf-pulse duration t_p. The values of $M(t_p,0)/(\mu_0 n)$ and $M(t_p,0,0)/(\mu_0 n)$ are the results of the integrations of the functions $I_1(\mathbf{r},t_p)$ and $I_2(\mathbf{r},t_p)$, respectively. For comparison, the value $H(t_p)=\ln|I_2(t_p)/I_1(t_p)|$, where the functions $I_1(t_p)$ and $I_2(t_p)$ are the integrals of the functions $B(\mathbf{r})\omega_1(\mathbf{r})I_1(\mathbf{r},t_p)$ and $B(\mathbf{r})\omega_1(\mathbf{r})I_2(\mathbf{r},t_p)$, respectively; (b) averaged squared gradients for the primary and for the stimulated echoes as a function of the rf-pulse duration t_p.

$$\ln\left|\frac{V(t_p,\tau_1,\tau_2)}{V(t_p,\tau_1)}\right| = \ln\left|\int B(\mathbf{r})\omega_1(\mathbf{r})I_2(\mathbf{r},t_p) \times \exp\left(-\gamma_p^2\mathbf{G}^2(\mathbf{r})Z_{\tau_1}(\tau_1+\tau_2)\right)\mathrm{d}v\right| - \ln\left|\int B(\mathbf{r})\omega_1(\mathbf{r})I_1(\mathbf{r},t_p)\exp\left(-\gamma_p^2\mathbf{G}^2(\mathbf{r})Z_{\tau_1}(\tau_1)\right)\mathrm{d}v\right| - \frac{\tau_2}{T_1}. \quad (7)$$

It can be transformed by a serial expansion of the exponents under the integrals with a follow-up integration:

$$\ln\left|\frac{V(t_p,\tau_1,\tau_2)}{V(t_p,\tau_1)}\right| \approx H(t_p) + \ln|1-\gamma_p^2\mathbf{G}_2^2 Z_{\tau_1}(\tau_1+\tau_2) + \cdots| - \ln|1-\gamma_p^2\mathbf{G}_1^2 Z_{\tau_1}(\tau_1)+\cdots| - \frac{\tau_2}{T_1}. \quad (8)$$

Here $H(t_p)=\ln|I_2(t_p)/I_1(t_p)|$. The functions $I_1(t_p)$ and $I_2(t_p)$ correspond to the integrals of the functions $B(\mathbf{r})\omega_1(\mathbf{r})I_1(\mathbf{r},t_p)$ and $B(\mathbf{r})\omega_1(\mathbf{r})I_2(\mathbf{r},t_p)$ over the volume. The parameters $\mathbf{G}_1^2(t_p)$ and $\mathbf{G}_2^2(t_p)$ are determined by the following expressions:

$$\mathbf{G}_1^2(t_p) = I_1^{-1}(t_p)\int B(\mathbf{r})\omega_1(\mathbf{r})I_1(\mathbf{r},t_p)\mathbf{G}^2(\mathbf{r})\,\mathrm{d}v, \quad (9)$$

$$\mathbf{G}_2^2(t_p) = I_2^{-1}(t_p)\int B(\mathbf{r})\omega_1(\mathbf{r})I_2(\mathbf{r},t_p)\mathbf{G}^2(\mathbf{r})\,\mathrm{d}v. \quad (10)$$

It is obvious that the functions $\mathbf{G}_1^2(t_p)$ and $\mathbf{G}_2^2(t_p)$ represent the averaged squared gradients in the sensitive volume with the excitation functions multiplied by $B(\mathbf{r})\omega_1(\mathbf{r})$ as weight functions. In general, they are pulse-length dependent functions which are different for the primary and for the stimulated echoes. If the function $\mathbf{G}(\mathbf{r})$ is constant, it follows from Eqs. (9) and (10) that the averaged squared gradients $\mathbf{G}_1^2(t_p)$ and $\mathbf{G}_2^2(t_p)$ are also constant and equal to each other and are independent of the pulse duration t_p. The real parts of these functions appear to be much larger than their imaginary parts for the portable NMR probe. They are shown in the diagram of Fig. 2b for the primary and the stimulated echo. For a pulse length $t_p = 7$ μs, which results in a maximum signal for the portable NMR probe (see Fig. 2a), they are almost equal for both echoes, which is mainly due to the fact that the gradient $\mathbf{G}(\mathbf{r})$ of the static magnetic field is almost constant in the sensitive volume. For the sake of simplicity it can therefore be stated that $\mathbf{G}_1^2(t_p)=\mathbf{G}_2^2(t_p)=\mathbf{G}^2=\text{const.}$ and $(\gamma_p\mathbf{G})^2 = 0.363\ \text{rad}^2/(\mu\text{s}^2\ \text{mm}^2)$ for $t_p = 7$ μs. This assumption allows one to simplify Eq. (8) by a serial expansion of the logarithmic function

$$\ln\left|\frac{V(t_p,\tau_1,\tau_2)}{V(t_p,\tau_1)}\right| \approx H(t_p) - \frac{\tau_2}{T_1} - \gamma_p^2\mathbf{G}^2(Z_{\tau_1}(\tau_1+\tau_2) - Z_{\tau_1}(\tau_1)) + \cdots \quad (11)$$

Further expansion terms are assumed to be much smaller in comparison to the first two. If the pulse-delay times are very short τ_1, $\tau_2 \to 0$, then the ratio between the stimulated and the primary echoes is equal to the ratio of the functions $I_2(t_p)$ and $I_1(t_p)$: $|V(t_p,\tau_1,\tau_2)/V(t_p,\tau_1)| = |I_2(t_p)/I_1(t_p)|$. Performing a further serial expansion for the function $\langle\mathbf{r}^2(|t''-t'|)\rangle$ at the points τ_1 and $\tau_1+\tau_2$ in Eq. (3), the expression $Z_{\tau_1}(\tau_1+\tau_2) - Z_{\tau_1}(\tau_1)$ can be represented as: $(\langle\mathbf{r}^2(\tau_1+\tau_2)\rangle - \langle\mathbf{r}^2(\tau_1)\rangle)\tau_1^2/6$. The last expression can be approximated as $\langle\mathbf{r}^2(\tau_2)\rangle\tau_1^2/6 + (d(\tau_2)-d(0))\tau_1^3$, where $6d(t) = \partial\langle\mathbf{r}^2(t)\rangle/\partial t$. For a linear time-dependence of the mean-square-displacement (MSD), $d(\tau_2)=d(0)$ and the term $(d(\tau_2)-d(0))\tau_1^3$ vanishes. For the diffusion in porous media we have $d(\tau_2)\approx d(0)$ for small times τ_2. If $\tau_1 \ll \tau_2$, then $(d(\tau_2)-d(0))\tau_1^3 \ll \langle\mathbf{r}^2(\tau_2)\rangle\tau_1^2/6$. It means that the expression $Z_{\tau_1}(\tau_1+\tau_2) - Z_{\tau_1}(\tau_1)$ can be approximated as $\langle\mathbf{r}^2(\tau_2)\rangle\tau_1^2/6$ for short and for long τ_2. This consideration suggests that the determination of the MSD from the ratio between the stimulated echo and the primary echo amplitudesshould provide a better accuracy for the MSD of liquid molecules in comparison to the determination of the

MSD from the ratio between the stimulated echo amplitudes and the initial magnetization. Besides this, measurements of the initial magnetization by NMR surface probe are difficult because of the dead time of the set-up after the application of the first rf-pulse. With $\mathbf{k} = \gamma_p \mathbf{G} \tau_1$ Eq. (11) can be written as

$$\ln \left| \frac{V(t_p, \tau_1, \tau_2)}{V(t_p, \tau_1)} \right| \approx H(t_p) - \frac{\tau_2}{T_1} - \frac{\langle \mathbf{r}^2(\tau_2) \rangle}{6} \mathbf{k}^2. \quad (12)$$

This is the expression for the logarithm of the ratio between the stimulated and the primary echo in the portable NMR probe. It contains the term $H(t_p) = \ln|I_2(t_p)/I_1(t_p)|$ that is responsible for the relaxation in inhomogeneous fields. Eq. (12) is used in the next section for the determination of the MSD of water molecules in porous media.

4. Experimental results

The theoretical considerations described above pointed out the feasibility of diffusion measurements with a portable NMR probe using three pulse-echo experiments. The duration of each pulse was 7 μs, which is much less than the delay between the first and the second pulse varying from 20 to 700 μs. The delay between the second and the third pulse was varied from 5 to 350 ms. In general, OSA NMR provides a poor signal-to-noise ratio (SNR) due to its low magnetic-field magnitude and homogeneity. To reach a satisfying precision, the number of the averaged experiments n should be between 50 and 500. Thus the measurement can last about 5–20 min.

The water diffusion in porous media was observed in two samples. Randomly packed glass beads of 100 μm diameter, characterized by a smooth surface and SiO_2 powder with grains showing a rough surface and an average size of 45 μm were filled with distilled water, so that it penetrated all cavities. The water level covered both media completely. The suspensions were let to rest for a few days under their own weight in order to get a stable density and to let the trapped air escape. Based on the absorbed water, volume porosities of $\varphi = 0.37$ for glass beads and $\varphi = 0.43$ for SiO_2 powder have been determined. Finally the samples were placed on the portable NMR probe such that the sensitive volume was located in the water-filled porous media.

Afterwards the MSD corresponding to a certain diffusion time τ_2 was determined from the measurement data by the procedure described in Section 3. For a constant time delay between second and third pulse, $\tau_2 = 5$ ms, the T_1 relaxation has a relatively small effect on the stimulated echoes. If the time-delay between the first and the second pulses τ_1 is varied, a series of primary and stimulated echoes are generated. This series is shown in Fig. 3a for the case of the water-filled SiO_2 powder.

To evaluate the MSD for a certain diffusion time τ_2, the values of the expression $-6\ln|V(t_p, \tau_1, \tau_2)/V(t_p, \tau_1)|$,

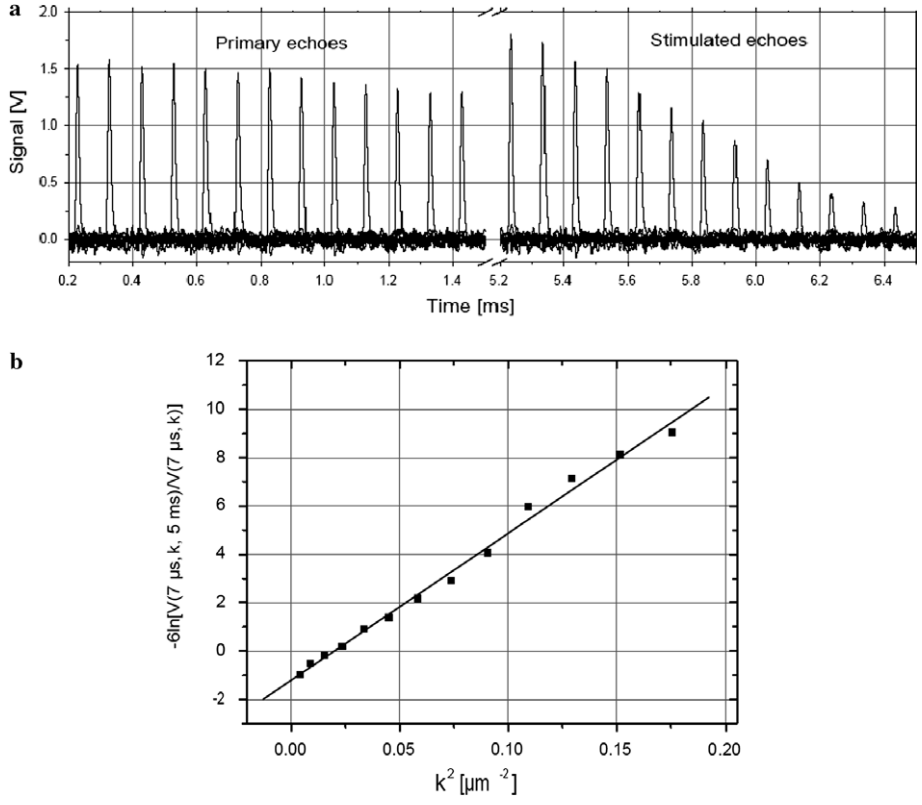

Fig. 3. Probe signals obtained from water-saturated SiO_2 powder; (a) set of primary and stimulated echoes with $\tau_2 = 5$ ms. The time delay τ_1 was varied in an interval between 100 and 700 μs; (b) value of $-6\ln|V(t_p, \tau_1, \tau_2)/V(t_p, \tau_1)|$ obtained from the echo amplitudes shown in (a) for $\tau_2 = 5$ ms and for different τ_1. Note that $6\ln|V(t_p, \tau_1, \tau_2)/V(t_p, \tau_1)|$ versus $\mathbf{k}^2$ is a straight line: $61[\mu m^2]\mathbf{k}^2 - 1.2$ (see Eq. (12)).

obtained from the measured echoes as a function of τ_1, are plotted versus $\mathbf{k}^2$ (see Fig. 3b). This plot is fitted by a straight line $A(\tau_2)\mathbf{k}^2 + R(\tau_2)$ with the slope $A(\tau_2)$ corresponding to $\langle \mathbf{r}^2(\tau_2)\rangle$. $R(\tau_2)$ represents the longitudinal relaxation and the influence of the field inhomogeneity $6(H(t_p) + \tau_2/T_1)$ for a single delay τ_2. If the measurement is repeated for several τ_2, the functional dependencies of $A(\tau_2)$ and $R(\tau_2)$ can be determined. The values of $A(\tau_2)$ divided by $6D\tau_2$ and $R(\tau_2)$ are shown in Figs. 4 and 5, respectively. Since $R(\tau_2)$ corresponds to $6(H(t_p) + \tau_2/T_1)$, the estimated values of $R(\tau_2)$ can be fitted by a straight line whose slope corresponds to the longitudinal relaxation rate $6/T_1$. A value of $T_1 = 310$ ms is obtained for the glass beads of 100 μm size and in case of the 45 μm SiO_2 powder T_1 is 62 ms (see Figs. 5a and b). The value of $A(\tau_2)$ corresponds to $\langle \mathbf{r}^2(\tau_2)\rangle$ which can be approximated for short times by the following expression [19,28–30]:

$$\frac{\langle \mathbf{r}^2(t)\rangle}{6Dt} \approx \left(1 - \frac{4}{9}\frac{S}{V}\sqrt{Dt}\right). \tag{13}$$

Short times mean the time intervals from the start of the experiment until the MSD begins to show asymptotic behavior.

Thus, the value of the specific surface S/V can be chosen in such a way that the curve, which is given by Eq. (13), fits best the time dependence $A(\tau_2)/6D\tau_2$ which was determined in the experiments. In this way a specific surface $S/V = 0.096\ \mu m^{-1}$ for the glass beads (see Fig. 4a) and $S/V = 0.21\ \mu m^{-1}$ for the SiO_2 powder is determined (see Fig. 4b). Presupposing spherical particles, the specific surface can be determined as $S/V = 6(1-\phi)/(d\phi)$ from the characteristic diameter d of the spheres and the porosity ϕ. By this way a value of $0.1021\ \mu m^{-1}$ is determined for the glass beads and $0.18\ \mu m^{-1}$ for the SiO_2 powder. These results are in good agreement with the values determined by the portable NMR surface probe. The specific surface value is linked with the relaxation time in porous media by the relation $\rho S/V = T_1^{-1}$, where ρ characterizes the surface ability to absorb proton magnetization. It follows from the above that the coefficient ρ is equal to 0.032 μm/ms and 0.08 μm/ms for the water-filled glass spheres and the water filled SiO_2 powder, respectively.

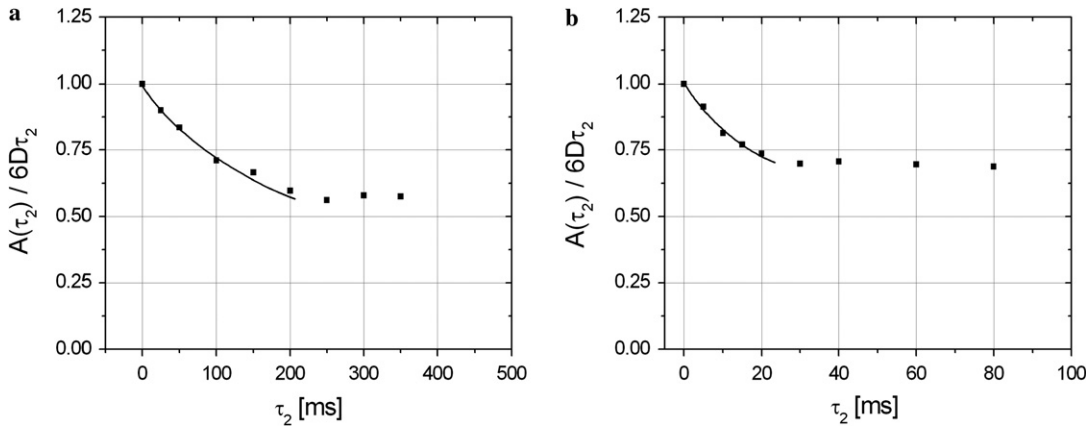

Fig. 4. Ratio between MSD of water molecules in porous medium and in an unrestricted volume; (a) for randomly packed glass spheres of 100 μm; (b) for SiO_2 powder of 45 μm.

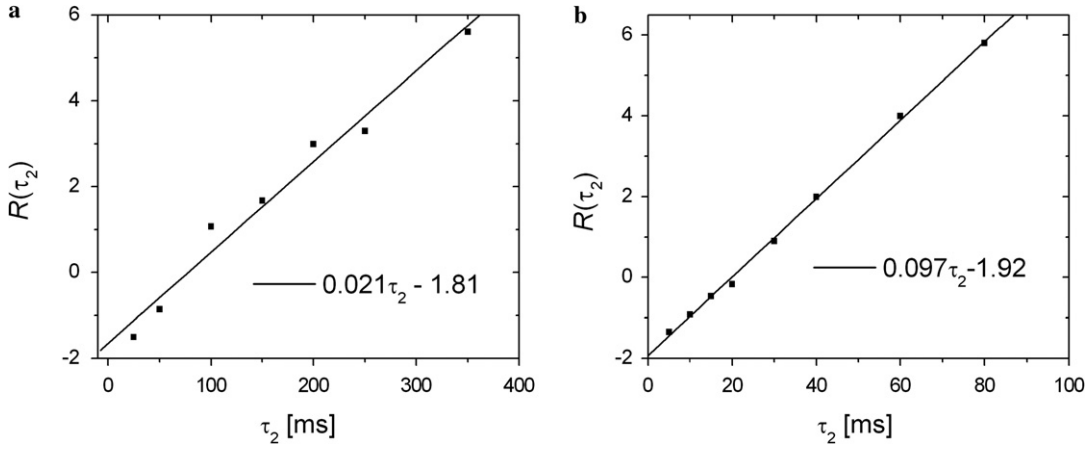

Fig. 5. Time dependence of $R(\tau_2)$; (a) in the glass-beads porous medium and (b) in SiO_2 powder. The slope of the fit straight line corresponds to the relaxation rate $1/T_1$.

It is also possible to determine the asymptotic value of the time-dependent diffusion coefficients in the long time limit $D(\infty)$ from the results described in Figs. 4a and b. The ratio $D(\infty)/D$ is 0.72 for the medium with the glass spheres and 0.6 for the SiO_2 powder.

The formation factor F which is defined as the ratio of the pure liquid conductivity to the conductivity of the liquid-filled porous medium, can be expressed using the asymptotic diffusion coefficient: $F^{-1} = \phi D(\infty)/D$ [28]. The formation factor can be linked with the permeability k of the porous medium by an empirical formula $k = \phi D F^{-1}\langle\tau\rangle$ [38]. Here $\langle\tau\rangle$ is a weighted average value of the relaxation time T_1. According to this formula the permeability of the medium with the glass spheres is 47.7 μm^2 and for the SiO_2 powder 17.6 μm^2.

5. Conclusion

Using a portable NMR probe, the recording of the time-behavior of the mean-squared displacement of the liquid molecules in porous media has been demonstrated. The specific surface of two porous media, here glass beads with a diameter of 100 μm and glass powder with a mean diameter of 45 μm, which were fully immersed in water, has been examined. The obtained values of the specific surface of the two tested porous samples are in good agreement with the calculated values. Based on this method the surface relaxivity ρ of an unknown porous medium can be determined, allowing one to eliminate the ambiguousness in relaxation-time analysis of porous media. Moreover, the portable NMR probe allows one to estimate the asymptotic value of the time-dependent diffusion coefficient $D(\infty)$, which is necessary to determine the formation factor F and the permeability k. The theoretical expression, which links the mean-squared displacement of diffusing molecules with the ratio between the stimulated echo and the primary echo amplitudes, has been calculated. This method should deliver a better accuracy for the determination of the mean-squared displacement in comparison to its determination from the ratio of the stimulated echo amplitude and the initial magnetization. Finally, this paper also offers a method for the approximation of the magnetic fields in the sensitive volume by polynomial expressions, which allows one to make simple and clear calculations of the echo amplitudes generated by the portable NMR probe.

Acknowledgments

One of the authors (A.M.) gratefully acknowledges the support by the graduate college "Materials for Efficient Energy Use" of the Material Science Department at the University of the Saarland. This graduate college was financed by the German Science Foundation. A.M. thanks also Professor Kröning, Director of IZFP, for his offer to join the IZFP for Ph.D. work.

Appendix A. Approximation of B(r) and $B_1(r,t)$ near the center of the sensitive volume

The planes x–z and x–y are the symmetry planes for the probe, $B(x,y,z)$ should be an even function with respect to the variable y and z: $B(x,y,z) = B(x,-y,z) = B(x,y,-z)$. This means that a series expansion of $B(x,y,z)$ cannot contain linear terms with respect to the variables y and z. Therefore the static magnetic field $B(x,y,z)$ or its proton Larmor frequency $\omega(x,y,z) = \gamma_p B(x,y,z)$ can be represented near the sensitive volume center as

$$\gamma_p B(x,y,z) = \gamma_p B_0 - b_x^{(0)} x - b_y^{(0)} y^2 + b_z^{(0)} z^2 \tag{A1}$$

The coefficients $b_x^{(0)}$, $b_y^{(0)}$, and $b_z^{(0)}$ are chosen such that the Eq. (A1) matches best the experimentally measured and numerically simulated field values. If distances are measured in millimeters, one gets $b_x^{(0)} = 0.6$ (rad/μs mm), $b_y^{(0)} = 7.4 \times 10^{-4}$ (rad/μs mm^2), and $b_z^{(0)} = 1.22 \times 10^{-3}$ (rad/μs mm^2). Eq. (A1) allows one to specify the shape of the sensitive volume located near the surface, which is determined by the equation $\gamma_p B(x,y,z) = \omega_0$. The thickness of the sensitive volume is proportional to the magnitude of the B_{1l} field close to this surface. In contrast to the standard NMR technique, the linearly polarized field $\mathbf{B}_{1l}(\mathbf{r},t)$ is not necessarily oriented orthogonally to the static magnetic field in the one-side probe. Note that it is only the transversal component which influences the spins during resonance: $\mathbf{B}_{1\perp}(\mathbf{r},t) = \mathbf{B}_{1l}(\mathbf{r},t) - (\mathbf{n}\cdot\mathbf{B}_{1l}(\mathbf{r},t))\mathbf{n}$. Here $\mathbf{n}$ is the unit vector along the field $\mathbf{B}(\mathbf{r})$. The field $\mathbf{B}_{1\perp}$ can be represented as the combination of two circularly polarized fields $\mathbf{B}_1(\mathbf{r},t)$ and $\mathbf{B}_1{}^*(\mathbf{r},t)$, which rotate with the angular speed $-\omega_0\mathbf{n}$ and $\omega_0\mathbf{n}$, respectively. The absolute value of both fields should be equal to the half of the absolute value of the field $\mathbf{B}_{1\perp}$, i.e., $|\mathbf{B}_1(\mathbf{r},t)| = |\mathbf{B}_1{}^*(\mathbf{r},t)| = |\mathbf{B}_{1\perp}(\mathbf{r},t)|/2$. The field $\mathbf{B}_1(\mathbf{r},t)$ can also be represented near the origin of the coordinate system as a polynomial function which reflects the symmetry of the coil. Since the symmetry axis of the coil is the x-axis, the field B_1 should depend on the distance from this axes $R = (y^2+z^2)^{1/2}$ and on the x-coordinate, $B_1(x,R)$. It is obvious that the field B_1 is maximal for a given x when $R \to 0$. This means that the derivative $\partial B_1(x,R)/\partial R = 0$ and the series expansion of the function cannot contain linear terms with respect to the variable R. Therefore the magnitude of the field B_1 or the proton precession frequency in this field $\omega_1(x,y,z) = \gamma_p B_1(x,y,z)$ can be represented as

$$\gamma_p B_1(x,y,z) = b^{(1)} - b_x^{(1)} x - b_{R1}^{(1)}(y^2+z^2) + b_{R2}^{(1)}(y^2+z^2)^2. \tag{A2}$$

Here, $b^{(1)} = 0.25595$ (rad/μs) is the magnitude of the rf-magnetic field at the coordinate origin. The coefficients $b_x^{(1)}$, $b_{R1}^{(1)}$, and $b_{R2}^{(1)}$ are chosen such that Eq. (A2) deviates from the experimental and numerical data by less than 5%. They are equal to $b_x^{(1)} = 1.25 \times 10^{-2}$ (rad/μs mm), $b_{R1}^{(1)} = 10^{-4}$ (rad/μs mm^2), and $b_{R2}^{(1)} = 1.27 \times 10^{-8}$ (rad/μs mm^4).

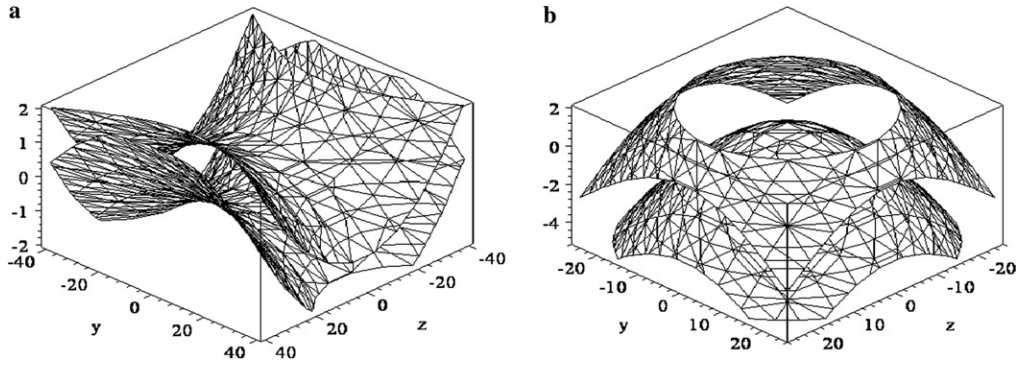

Fig. 6. Equal amplitude surfaces for the magnetic fields of the portable NMR probe near the center of the sensitive volume. The numbers along the x-axes and y-axes represent mm. (a) For the upper surface the static magnetic field amplitude is $\gamma_p B(x,y,z) = \gamma_p B_0 - 0.5$ (rad/μs). For the lower surface $\gamma_p B(x,y,z) = \gamma_p B_0 + 0.5$ (rad/μs). (b) For the upper surface the rf-magnetic field amplitude is equal to $\gamma_p B_1(x,y,z) = 0.25$ (rad/μs). For the lower surface: $\gamma_p B_1(x,y,z) = 0.2$ (rad/μs).

Eqs. (A1) and (A2) with the above determined gradient are used to calculate the magnitude of the field distributions near the coordinate origin, and hence the sensitive volume. The surfaces of equal amplitude for the static field $B(x,y,z)$ are plotted in Fig. 6a. The difference between the $\gamma_p B$ values on the lower and on the higher surfaces is approximately equal to the quadruple magnitude of the rf-field: $4B_1(0,0,0)$. The main part of the sensitive volume is enclosed between these two surfaces. The graph of the rf-field B_1 is shown in Fig. 6b. It represents the extent of the sensitive volume in the horizontal plane.

Appendix B. Calculation of the magnetization rotation during rf-pulses

The rotation during a rf-pulse of length t_p around the deviated axis by an angle $\alpha(\mathbf{r},t_p) = -\gamma_p(\Delta B^2(r) + B_1^2(\mathbf{r}))^{1/2} t_p$ can be described by the rotation matrix which depends on the angles φ, θ, and α

$$P(\varphi,\vartheta,\alpha) = R_z(\varphi)R_y(-\vartheta)R_x(\alpha)R_y(\vartheta)R_z(-\varphi). \tag{B1}$$

Here the matrices R_x, R_y, R_z, represent the standard rotation about the x, y, and z axis, respectively. The angle $\vartheta(\mathbf{r})$ is determined by the equation: $\tan\vartheta(\mathbf{r}) = \Delta B(\mathbf{r})/B_1(\mathbf{r})$. φ is phase of the rf-pulse. Using Eq. (B1) and the standard expression for the R_x, R_y, R_z, the rotation matrices of the rf-pulses at the point $\mathbf{r}$, $P(\varphi,\vartheta(\mathbf{r}),\alpha(\mathbf{r},t_p))$, can be explicitly calculated. In Eq. (B1) the transformation $R_y(\theta)R_z(-\varphi)$ puts the effective field-precession axis along the x-axis of the new coordinate system. $R_x(\alpha)$ is responsible for spin precession during the rf-pulse, and $R_z(\varphi)R_y(-\theta)$ returns the rotated vector to the old coordinate system. For the most common cases of x or y pulses, when the phases are $\varphi = 0$ or $\varphi = \pi/2$, respectively, the following notations are used $P_x(\mathbf{r},t_p) \equiv P(0,\vartheta(\mathbf{r}),\alpha(\mathbf{r},t_p))$ and $P_y(\mathbf{r},t_p) \equiv P(\pi/2, \vartheta(\mathbf{r}),\alpha(\mathbf{r},t_p))$.

$$P_x(\mathbf{r},t_p) \equiv P\big(0,\vartheta(r),\alpha(\mathbf{r},t_p)\big) = \begin{pmatrix} I(\mathbf{r},t_p) & -o(\mathbf{r},t_p) & O(\mathbf{r},t_p) \\ o(\mathbf{r},t_p) & c(\mathbf{r},t_p) & -s(\mathbf{r},t_p) \\ O(\mathbf{r},t_p) & s(\mathbf{r},t_p) & C(\mathbf{r},t_p) \end{pmatrix},$$

$$P_y(\mathbf{r},t_p) \equiv P\Big(\frac{\pi}{2},\vartheta(r),\alpha(\mathbf{r},t_p)\Big) = \begin{pmatrix} c(\mathbf{r},t_p) & -o(\mathbf{r},t_p) & s(\mathbf{r},t_p) \\ o(\mathbf{r},t_p) & I(\mathbf{r},t_p) & O(\mathbf{r},t_p) \\ -s(\mathbf{r},t_p) & O(\mathbf{r},t_p) & C(\mathbf{r},t_p) \end{pmatrix}.$$

$I(\mathbf{r},t_p)$, $O(\mathbf{r},t_p)$, $o(\mathbf{r},t_p)$, $C(\mathbf{r},t_p)$, $c(\mathbf{r},t_p)$, $s(\mathbf{r},t_p)$ are determined by the following expressions:

$$I(\mathbf{r},t_p) = \cos^2\vartheta(\mathbf{r}) + \cos\alpha(\mathbf{r},t_p)\sin^2\vartheta(\mathbf{r}),$$
$$o(\mathbf{r},t_p) = \sin\alpha(\mathbf{r},t_p)\sin\vartheta(\mathbf{r}),$$
$$O(\mathbf{r},t_p) = \big(1-\cos\alpha(\mathbf{r},t_p)\big)\sin\vartheta(\mathbf{r})\cos\vartheta(\mathbf{r}),$$
$$c(\mathbf{r},t_p) = \cos\alpha(\mathbf{r},t_p),$$
$$C(\mathbf{r},t_p) = \cos\alpha(\mathbf{r},t_p)\cos^2\vartheta(\mathbf{r}) + \sin^2\vartheta(\mathbf{r}),$$
$$s(\mathbf{r},t_p) = \sin\alpha(\mathbf{r},t_p)\cos\vartheta(\mathbf{r}).$$

In the case when $\Delta B(\mathbf{r}) \ll B_1(\mathbf{r})$ or $\vartheta = 0$ across the sample, the following holds $O = o = 0$, $I = 1$, $C = c = \cos\alpha$, $s = \sin\alpha$ with $\alpha = -\omega_1 t_p$, and the matrices $P_x(\mathbf{r},t_p)$, $P_y(\mathbf{r},t_p)$ are transformed into the standard matrices $R_x(\alpha)$ and $R_y(\alpha)$, respectively.

References

[1] R.L. Kleinberg, Encyclopedia of Nuclear Magnetic Resonance, Ch. Well logging, vol. 8, Wiley, Chichester, 1996, pp. 4960–4969.
[2] See collected papers in: J.A. Jackson (Ed.), The history of NMR well loggingConc. Magn. Reson. 13 (2001) 340–411 (special issue).
[3] G.A. Matzkanin, Applications of nuclear magnetic resonance to the NDE of composites, in: D.W. Moore, G.A. Matzkanin (Eds.), Proc. 14th Symp. NDE, Am. Soc. Non-Destructive Testing, San Antonio, 1983, pp. 270–286.
[4] B. Wolter, ^{1}H-NMR Verfahren in Aufsatztechnik zur zerstörungsfreien Charakterisierung zementgebundener und organischer poröser Werkstoffe", Ph.D. thesis, Naturwissenschaftlich—Technische Fakultät III, Universität des Saarlandes and IZFP report No. 010162-TW, 2001.
[5] B. Blümich, P. Blümler, G. Eidmann, A. Guthausen, R. Haken, U. Schmitz, K. Seito, G. Zimmer, The NMR mouse: construction, excitation and applications, Magn. Reson. Imaging 16 (1998) 479–484.

[6] G. Eidmann, Entwicklung und Anwendung eines NMR Oberflächenscanners: die NMR—Mouse, PhD thesis, Fakultät für Mathematik, Informatik und Naturwissenschaften, RWTH Aachen, and Shaker Verlag, Aachen, 1998.
[7] B. Wolter, A. Hartwig, Zerstörungsfreie NMR-Aufsatztechnik: Anwendungsbeispiele und Möglichkeiten, Adhäsion Kleben & Dichten 45 (2001) 34–38.
[8] K. Kremer, H. Kühl, B. Blümich, J. Seitzer, F.P. Schimtz, NMR-MOUSE® ermöglicht Online-Qualitätskontrolle im KFZ-Bau, Adhäsion, Kleben und Dichten 46 (2002) 32–36.
[9] B. Wolter, G. Dobmann, N. Surkowa, F. Kohl, Kernresonanz in Aufsatztechnik, Technisches Messen 69 (2002) 43–48.
[10] S. Sharma, F. Casanova, W. Wache, A. Segre, B. Blümich, Analysis of historical porous building materials by the NMR-MOUSE®, Magn. Reson. Imaging 21 (2003) 249–255.
[11] D. Capitani, N. Proietti, A.L. Segre, Non invasive analysis by unilateral NMR applied to the cultural heritage presented at "4th Colloquium on Mobile NMR", Aachen, Germany, 2004, unpublished.
[12] P.J. Prado, Single-sided imaging sensor, Magn. Reson. Imaging 21 (2003) 397–400.
[13] P.J. Prado, NMR hand-held moisture sensor, Magn. Reson. Imaging 19 (2003) 505–508.
[14] P.J. Prado, B. Blümich, U. Schmitz, One-dimensional imaging with a palm-size NMR-probe, J. Magn. Reson. 144 (2000) 200–206.
[15] L. Grunin, B. Blümich, Resolving chemical shift spectra with a low-field NMR relaxometer, Chem. Phys. Lett. 397 (2004) 306–308.
[16] J. Perlo, V. Demas, F. Casanova, C.A. Meriles, J. Reimer, A. Pines, B. Blümich, High-resolution NMR spectroscopy with a portable single-sided sensor, Science 308 (2005) 1279.
[17] P.T. Callaghan, Principles of Nuclear Magnetic Resonance Microscopy, Clarendon Press, Oxford, 1991.
[18] R. Kimmich, NMR Tomography, Diffusometry, Relaxometry, Springer Verlag, Berlin, 1997.
[19] P.N. Sen, Time-dependent diffusion coefficient as a probe of geometry, Conc. Magn. Reson. 23A (2004) 1–21.
[20] A. Marko, B. Wolter, Diffusion studies in porous media with the "inside-out" technique, Magn. Reson. Imaging 21 (2003) 363–364.
[21] E.L. Hahn, Spin echoes, Phys. Rev. 80 (1950) 580–594.
[22] H.Y. Carr, E.M. Purcell, Effects of diffusion on free precession in nuclear magnetic resonance experiments, Phys. Rev. 94 (1954) 630–638.
[23] E.O. Stejskal, J.E. Tanner, Spin diffusion measurements: spin echoes in the presence of a time-dependent field gradient, J. Chem. Phys. 42 (1965) 288–292.
[24] K.R. Brownstein, C.E. Tarr, Importance of classical diffusion in NMR studies of water in biological cells, Phys. Rev. A 19 (1979) 2446.
[25] M.D. Hürlimann, Diffusion and relaxation effects in general stray field NMR experiments, J. Magn. Reson. 148 (2001) 367–378.
[26] M.D. Hürlimann, L. Venkataramanan, Quantitative measurement of two-dimensional functions of diffusion and relaxation in grossly inhomogeneous fields, J. Magn. Reson. 157 (2002) 31–42.
[27] M.D. Hürlimann, L. Venkataramanan, C. Flaum, The diffusion-spin relaxation time distribution function as an experimental probe to characterize fluid mixtures in porous media, J. Chem. Phys. 117 (2002) 10223–10232.
[28] P.P. Mitra, P.N. Sen, Effects of microgeometry and surface relaxation on NMR pulsed-field-gradient experiments: Simple geometries, Phys. Rev. B 45 (1992) 143–156.
[29] P.P. Mitra, P.N. Sen, L.M. Schwartz, P. Doussel, Diffusion propagator as a probe of the structure of porous media, Phys. Rev. Lett. 68 (1992) 3555–3558.
[30] P.P. Mitra, P.N. Sen, L.M. Schwartz, Short-time behavior of the diffusion-coefficient as a geometrical probe of porous media, Phys. Rev. B 47 (1993) 8565–8574.
[31] A. Marko, B. Wolter, W. Arnold, Magnetization density calculation for diffusing spins, Phys. Rev. B69 (2004) 184424-1–184424-8.
[32] M. Klein, R. Fechete, D.E. Demco, B. Blümich, Self-diffusion measurements by a constant-relaxation method in strongly inhomogeneous magnetic fields, J. Magn. Reson. 164 (2003) 310–320.
[33] T.J. Norwood, R.A. Quilter, A robust NMR method for studying diffusion, J. Magn. Reson. 97 (1992) 99–110.
[34] M.D. Hürlimann, D. Griffin, Spin dynamics of Carr–Purcell–Meiboom–Gill like sequences in grossly inhomogeneous B_0 and B_1 fields and application to NMR well logging, J. Magn. Reson. 143 (2000) 120–135.
[35] Y.-Q. Song, Categories of coherence pathways for the CPMG sequence, J. Magn. Reson. 157 (2002) 82–91.
[36] F. Balibanu, K. Hailu, R. Eymael, D.E. Demco, B. Blümich, Nuclear magnetic resonance in inhomogeneous magnetic fields, J. Magn. Reson. 145 (2000) 246–258.
[37] A. Marko, Anwendungsmöglichkeiten der 1H-Kernresoanz-Methode zur hydrologischen Charakterisierung poröser Gesteine, Ph.D. Thesis, Naturwissenschaftlich—Technische Fakultät III, Universität des Saarlandes, 2005 and IZFP report No. 050115-TW, 2005.
[38] L.M. Schwartz, N. Martys, D.P. Bentz, E.J. Garboczi, S. Torquato, Cross property relations and permeability estimation in model porous media, Phys. Rev. E 48 (1993) 4584–4591.